Journal Pre-proof

Observational analysis of two waterspouts in northwestern Italy using an OPERA Doppler radar

Mario Marcello Miglietta, Ken'ichiro Arai, Kenichi Kusunoki, Hanako Inoue, Toru Adachi, Hiroshi Niino

PII: S0169-8095(19)31001-4

DOI: https://doi.org/10.1016/j.atmosres.2019.104692

Reference: ATMOS 104692

To appear in: *Atmospheric Research*

Received date: 2 August 2019

Revised date: 19 September 2019

Accepted date: 24 September 2019

Please cite this article as: M.M. Miglietta, K. Arai, K. Kusunoki, et al., Observational analysis of two waterspouts in northwestern Italy using an OPERA Doppler radar, *Atmospheric Research*(2018), https://doi.org/10.1016/j.atmosres.2019.104692

Observational analysis of two waterspouts in northwestern Italy using an OPERA Doppler radar

Mario Marcello Miglietta

ISAC-CNR, Padua/Lecce, Italy

Ken'ichiro Arai, Kenichi Kusunoki, Hanako Inoue, Toru Adachi

Meteorological Research Institute, Japan Meteorological Agency, Tsukuba, Japan

Hiroshi Niino

AORI, University of Tokyo, Tokyo, Japan

Keywords: Waterspout, Doppler radar, Tornado Vortex Signature

ABSTRACT

Data from a C-band dual-polarization Doppler radar are used to analyze the evolution of two waterspouts in the Mediterranean Sea, observed in front of the coastal city of Sanremo, northwestern Italy, on December 1, 2017. The integration of reflectivity and wind data allows to identify a mesocyclone aloft, and a Doppler velocity couplet, corresponding to a change in wind speed and/or direction in two adjacent individual pixels on radar display, at two different elevations. The latter signal is classified as a Tornado Vortex Signature, suggesting the presence of two vortices moving northward through the coast near Sanremo. The reconstructed paths agree well with the damage and eyewitness evidence. Radar data also suggest that the two waterspouts developed in the region of convergence separating the incoming cold air from the warm and moist inflow.

1. Introduction

Following the AMS glossary, the term waterspout denotes, in general, any tornado over a body of water; in its most common use, it represents a non-mesocyclonic tornado over water. It consists of "an intense columnar vortex (usually containing a funnel cloud) that occurs over a body of water and is connected to a cumuliform cloud". Some field campaigns in the Florida Keys provided a unique opportunity to learn more about their structure and wind fields; consequently, Golden (1974a, b) proposed a waterspout life cycle based on five stages.

Waterspouts occur most frequently in the subtropics during the warm season, but are not exclusive of this region. The Mediterranean coasts from Spain to Italy, from Greece up to the Black Sea, with their numerous islands and peninsulas, represent an extremely complex topography, favorable for waterspout triggering (Sioutas and Keul, 2007).

Waterspouts generally form beneath lines of growing cumulus congestus, often in environments characterized by weak vertical wind shear. Differently from mesocyclonic tornadoes, they do not form by reorientation and generation of vorticity within a downdraft; like non-mesocyclonic tornadoes over land (*landspouts*; Bluestein, 1985), they usually develop in intensifying preexisting small-scale surface vortices (called *misocyclones*). Thus, they form along air mass boundaries with large wind shifts associated with local maxima of low-level horizontal wind shear and vertical vorticity (Wakimoto and Wilson, 1989; Lee and Wilhelmson, 1997a, b), e.g. along low-level convergence lines, frontal lines, sea-breeze fronts. Multiple spouts are sometimes observed simultaneously along these lines (Sioutas et al., 2013).

Waterspouts may also form in sheared environments, where the tilting of environmental horizontal vorticity into the vertical may generate vortices, as it happens for supercells. In these cases, a rotating updraft would provide a different source of vorticity from that associated with preexisting low-level vortices. Over the Ionian Sea, a mechanism for generation of mesocyclonic waterspouts was identified in the tilting of horizontal rolls moving over the sea beneath convective cells advected offshore after being triggered by the rough coastal orography (Miglietta and Rotunno, 2016; Miglietta et al., 2017a, b).

A rotating updraft is generally the main source of vorticity for waterspouts associated with well-developed cumulus congestus or small cumulonimbus clouds. In these cases, spouts tend to form in the vicinity of gust-front outflows from nearby rain showers; the strong convergence enhances the updrafts and concentrates the vorticity into a narrow vortex below cloud base (Simpson et al., 1986).

The literature on waterspouts is not extensive. Only after the late 1960s and early 1970s, waterspouts started to be investigated in detail mainly by means of in situ airborne measurements in the Florida Keys. Further progress was made by means of Doppler radar, which offered the possibility to investigate waterspout environments more in detail. The combination of radar data with observations of the near storm environment represents one of the best methods for waterspout forecasting (Markowski and Richardson, 2010).

The first case of a Doppler-observed mesocyclone, associated with a damaging waterspout in Florida, was discussed in Golden and Sabones (1991). In that case, the mesocyclone was only detected in the lower levels of the parent thunderstorm, at the southwest end of a line. Wakimoto and Lew (1993) analyzed a waterspout that developed from a relatively small cumulus cloud, collecting detailed Doppler radar information on the parent cloud. The waterspout formed during the cumulus growth stage and dissipated when a rain shower reached the surface. Although the waterspout was only 15 km far from the radar, the small width of the vortex prevented from detecting a pronounced rotational couplet below 1 km MSL. Surprisingly, the largest azimuthal shear within the cloud was recorded during the dissipation of the waterspout. An airborne Doppler radar allowed the high-resolution analysis of the velocity and vorticity structure of a waterspout parent storm in the Pacific Ocean (Verlinde, 1997). The observations suggested the presence of a source of vorticity in the low-levels. Collins et al. (2000) estimated the radial velocity of a waterspout in Florida from a WSR-88D radar, identifying the vertical vorticity source in a region of near-surface horizontal shear, about 30 min before tornadogenesis. This case demonstrates that a non-mesocyclonic tornado may be anticipated before a “tornado vortex signature” appears, providing sufficient lead time to

operational forecasters. On May 31, 2007, Doppler radar observations and field surveys revealed the detailed structures of the funnel and of the parent cloud for a waterspout occurred near Tokyo (Sugawara and Kobayashi, 2008). The waterspout formed over a wind shear zone, favoring the development of an anticyclonic vortex.

The combination of satellite and radar images allowed to identify the development of the parent cells associated with an outbreak of five waterspouts near Barcelona on September 7, 2005, responsible for 9 M€ of damage after moving inland. The vortices developed along a mesoscale convergence line in a highly sheared and relatively low buoyant environment (Bech et al., 2007). A three-dimensional coherent Doppler lidar and C-band Doppler radar were able to detect a cyclonic waterspout very close to the sea surface near Ikeshima island, Japan, on 21 December 2010. Data analysis allowed to identify the presence of the waterspout and two sub-scale vortices along a gust front ahead of the parent storm (Fujiwara and Fujiyoshi, 2014). Misovortices frequently form over the Japan Sea during wintertime cold air outbreaks and move inland at later times. Kato et al. (2015) analyzed the temporal changes in the intensity and tilt of twelve different misovortices using an X-band Doppler radar, showing a rapid decay and increased tilt soon after landfall. Van Den Broeke and Van Den Broeke (2015) used polarimetric radar observations to analyze the waterspout-producing convection during an outbreak of four waterspouts produced by a convective cell over the western Lake Michigan on 12 September 2013. The storm initiated along a boundary north of a meso-low in a low-level cold-air advection regime, and developed supercell characteristics once the second waterspout was in progress.

In the present study, we use the data from a C-band dual-polarization Doppler radar to infer information on two waterspouts observed in the Mediterranean Sea, in front of the coastal city of Sanremo, northwestern Italy, on December 1, 2017. The interest for this case study is related to the radar coverage of the event, which allows one of the first detailed analyses of a waterspout in the Mediterranean using Doppler radar data. The paper is organized in the following way. The geographic environment where the waterspouts developed and the synoptic features during the case

study are discussed respectively in Section 2 and 3. Data and methods used for the analysis are introduced in Section 4, while results are discussed in Section 5. Conclusions are drawn in Section 6.

2. Geographic environment

Liguria is a narrow, arc-shaped administrative and geographic region of northwestern Italy, located between relatively steep, although not very high mountains (peaks around 2000 m) on its northern side (the southern tip of the Alps and the northern part of the Apennines chain) and the Mediterranean Sea on its southern side (Fig. 1). Its coastline (330 km long) is exposed to heavy rainfall episodes almost every year, especially during autumn, which are mainly associated with intense quasi-stationary convective systems (Cassola et al., 2016). These systems generally develop due to the convergence between a cold air outflow, moving from the north, with warm and moist southerly flow offshore, fed by intense sensible and latent surface fluxes (Buzzi et al., 2014; Fiori et al., 2014; Cassola et al., 2016). The balance between the two flows determines the position of the mesoscale convergence line over the sea, which, together with the lifting produced by the mountains close to the coast, control the onset of severe convection.

Additionally, Liguria is exposed to the frequent occurrence of waterspouts. In a recent study over Italy (Miglietta and Matsangouras, 2018), Liguria appears as a hotspot area for waterspouts, with an average of 9.3 events and a density of almost 3 events per 100 km of coastline per year, much higher than the average of 0.92 recorded over the whole Italian coastlines; the spouts concentrate mainly in autumn and summer, with a slight prevalence of episodes in the former season. In December, waterspouts are not rare in Liguria: 6 occurrences (2 of which in front of Sanremo) were recorded over a total of 93 vortices in 10 years (2007-2016; Miglietta and Matsangouras, 2018). However, the landfall is very unusual in this month[1].

The region has also the highest density of tornadoes of all Italian (geographic and administrative) regions, with an average of 3.88 events per 10.000 km^2 per year, i.e. about the value of Florida, the

[1] Only two other landfalls in December are recorded in the dataset of tornadoes over Italy managed by the first author of the present paper, respectively in 2000 and 2017.

state in the U.S. with the highest tornado rate (Simmons and Sutter, 2011). These tornadoes are generally weak vortices, originated as waterspouts that survive just a few hundred meters after landfall, and only rarely exceed level 0 in Enhanced Fujita scale (EF-scale; McDonald and Mehta, 2006): five EF1 events were reported from 2007 to 2016, while vortices stronger than EF1 were not recorded (Miglietta and Matsangouras, 2018).

The presence of the Gulf of Genoa, one of the main cyclogenetic region in the Mediterranean (Tibaldi et al, 1990), may partly explain the higher waterspout density compared to the rest of Italy and other Mediterranean regions. A study is in progress to better identify the characteristics of tornado-spawning extratropical cyclones in Italy, in a way similar to what recently done for USA and Japan (Tochimoto and Niino, 2016, 2018).

3. Case study

Two waterspouts were reported in the Mediterranean Sea, in front of the city of Sanremo (43.812°N, 7.780°E), along the western coast of Liguria region, at around 1130 UTC (1230 LST) on December 1, 2017. The most intense waterspout made landfall near the city center, causing damages to some houses at around 1140 UTC and injuring two persons. The strength of the vortex was estimated as EF0. Since the waterspouts occurred in a populated area during daytime, they were recorded by several cameras, which made available several pictures and videos on the web (e.g., https://www.quotidiano.net/cronaca/foto/tromba-marina-sanremo-1.3574190); the images show that they developed at the border between cloud-covered and cloud-free areas. Although the vortices were relatively weak, they are analyzed here because of the radar coverage of the event (see Section 4), which makes this case study appropriate to apply vortex detection techniques for the first time -to our knowledge- in the Mediterranean.

The synoptic conditions associated with the case study are analyzed hereafter. The Climate Forecasting System reanalysis (CFS; Saha et al., 2010) at 1200 UTC, 1 December 2017 shows that the central Mediterranean was affected by a wide upper-level cyclonic circulation centered over the

Baltic Sea, elongated in meridional direction toward northern Africa (Fig. 2, top). The cyclonic circulation remained blocked in the area, being confined between the Azores High to the west (extending northward up to the British islands) and the Siberian High to the east. A weak minimum in mean sea level pressure is present over the central Mediterranean basin, which the UK Met Office Bracknell weather map (Fig. 2, bottom) identifies more exactly between Liguria and the northern Tyrrhenian Sea. The presence of a cold front, extending to the west of Liguria region, denotes the intrusion of cooler air in the low levels over the western Mediterranean.

The closest radiosounding station to Sanremo is in Cuneo Levaldigi, located about 80 km to the north (Fig. 1). Figure 3 shows the vertical profile at 1200 UTC, 1 December 2017. Although the environment retrieved by the sounding is representative of the western Po Valley, thus it may differ significantly, especially in the low levels, from the coastal environment, some useful pieces of information can be extracted. In particular, the estimated tropopause height of about 5500 m height is consistent with the radar echo distribution (see Section 5), confirming that convective clouds cannot develop to high altitude in this event due to the low tropopause.

For the sake of comparison with the climatology of waterspouts in other Mediterranean regions, the vertical wind differences for the present case study are compared with the data for Catalonia (Rodríguez and Bech, 2017): the value is close to the climatological mean in the 0-1 km (5.5 m s^{-1}) and 0-3 km layer (9.5 m s^{-1}), while it is near the 75th percentile in the 0-6 km layer (22 m s^{-1})[2]. Similar considerations can be drawn in comparison with the waterspouts in the eastern Adriatic (Renko et al., 2016). In contrast, the vertical wind shear is weaker in all layers compared with the climatological mean for F0 vortices in Italy (Giaiotti et al., 2007); however, the latter dataset includes not only waterspouts, but also tornadoes over land.

The very low values of CAPE in Fig. 3 are consistent with the results for the southern Aegean Sea of Greece in winter (Matsangouras et al., 2017). However, the cold temperature up to 800 hPa and the inversion just above (Fig. 3) are indicative of a cold pool, which generally persists over the

[2] The intense deep layer shear is due to an upper level southwesterly jet stream over the central Mediterranean.

Po Valley in wintertime; hence, the temperature profile, and consequently CAPE, cannot be considered as representative of the real environment over the sea.

4. Data and methods

The present case is analyzed by means of the weather radar located in Settepani mountain (44.245897°N, 8.197409°E), about 60 km northeast of Sanremo, at an elevation of 1364 m (Fig. 4). This is a C-band dual-polarization Doppler radar, whose specifications are provided in Tab. 1. The Nyquist velocity V_N, which determines the maximum velocity that can be identified without aliasing, is given by: $V_N = \frac{1}{4}\lambda\, PRF$ (where λ is the wavelength and PRF the pulse repetition frequency), which is equal to 11.8 m s^{-1} for this radar.

MAXIMUM RANGE	360 km
RANGE RESOLUTION	500 m
HEIGHT OF THE ANTENNA	1395 m.a.s.l.
DIAMETER	4.2 m
BEAM WIDTH	0.939°
WAVELENGTH (λ)	5.333 cm
GAIN	44.9 dB
PULSE REPETITION FREQUENCY (PRF)	882 Hz
FREQUENCY	5.64 GHz
NUMBER OF BINS	345
NUMBER OF RAYS	360
NYQUIST VELOCITY	11.76 m/s

Tab. 1: Monte Settepani Doppler radar specifications.

The observational mode of the Settepani mountain radar consists of a volume scan with 8 elevation angles every 5 minutes. The time for scanning and the different elevation angles are shown in Fig. 5. The highest two beams scan the atmosphere with an angle respectively of 28.5° and 15.0° above ground, thus they are too high to represent the troposphere above Sanremo; in contrast, the other beams (at an elevation EL respectively of 6.4°, 4.0°, 2.1°, 0.7°, and -0.3°) scan most of the troposphere above the point where the waterspouts were seen. In particular, the lowest beam EL = -0.3° (corresponding to about 1300 m height above Sanremo) exploits the high elevation of the radar site to scan the troposphere at low levels without being significantly shadowed by the

orography in the area (the topographic profile from the radar site to Sanremo is shown in the lower side of Fig. 5).

The radar site belongs to OPERA (Operational Programme for the Exchange of Weather Radar Information; Huuskonen et al., 2014), the radar program of EUMETNET. OPERA provides a European platform wherein high-quality pan-European weather radar composite products are developed on an operational basis and expertise in weather radar is exchanged across Europe. Data is provided in HDF format; in this way, radar data can be read without using a proprietary decoding tool. Dealiasing of velocity data is generated automatically; in addition, manual correction is performed for dealiasing failure of velocity data. In this way, a vertical wind profile in Sanremo area is virtually provided.

In the following, the peak tangential velocity of the vortex is calculated as one-half the difference between the Doppler velocity maximum and minimum; the core diameter of the vortex is defined as the distance between the locations of the velocity maximum and minimum.

5. Results

The plan position indicator (PPI) scans at different times (increasing from top to bottom) and different EL (decreasing from left to right) are shown in Fig. 6. At 1031-1032 UTC (Fig. 6, top), the radar images show the presence of a rainband in the lower three beams, spanning the lowest 4 km of the troposphere above Sanremo. The rainband, elongated from south-east to north-west, approaches the Ligurian coast from the sea, with reflectivity values reaching a maximum of about 40 dBZ at EL = 0.7° (corresponding to about 2250 m near Sanremo). In the next 30 minutes (not shown), the rainband becomes more intense (maximum reflectivity values above 45 dBZ), and develops into a wider and deeper precipitation system (extending up to EL=4.0°, at about 6 km height).

This precipitation system moves east-northeastward, and spawns the waterspout that makes landfall near Sanremo. Near the time of the passage of the waterspout over Sanremo, at around 1130 UTC (Fig. 6, middle), the reflectivity values further increase, with a maximum of about 50

dBZ detected at EL = 0.7° and EL = 2.1°. A small signature of an elongated pattern of high reflectivity is also apparent at these two levels inland, on the southwestern side of the cell, very close to the coastline; the feature resembles a hook echo (van Tassel, 1955; Markowski, 2002), which is one of the classic hallmarks of tornado-producing supercells.

By 1201-1202 UTC (Fig. 6, bottom) the system has changed its direction of displacement, moving southeastward and intensifying up to 55 dBZ. In the low levels, an east-west elongated line-shaped maximum can be identified, suggesting a change in the nature of the system, possibly due to the inflow of colder air pushing from the northern side. After 30 minutes, the system proceeds further southeastward, still showing an arc-like pattern in its extreme southern tip (not shown); at this time, the highest reflectivity values are located completely offshore. Since the highest elevation angle for which the radar echo can be identified above Sanremo area is about 4.0°, one may infer that the echo top of the tornado-spawning cell during the whole lifetime is at about 6 km height, consistent with the vertical profile shown in Fig. 3.

The PPI at 0.7° elevation angle (with starting azimuth of 87.5°) and the Doppler radar data after dealiasing are shown in Fig. 7. A strong radar echo (values above 50 dBZ) can be identified in the reflectivity field at 1147 UTC (Fig. 7a), with a bounded weak echo region (BWER; Markowski, 2002), east of the hook echo. The latter region appears at the center of a mesocyclone, showing inbound (southwesterly) winds of 25.9 m/s offshore on its eastern side, and outbound (northeasterly) winds of 1.3 m/s in correspondence with the maximum reflectivity inland. The black circle in the upper-right panel of Fig. 7 shows the location of the mesoscale vortex, which has been identified subjectively. This pattern is even more apparent 15 minutes later (at 1202 UTC), when the outbound velocity reaches nearly 10 m/s (Fig. 7b, right).

Figure 7 shows that the integration of reflectivity with wind data is helpful in order to identify a mesocyclone aloft. The eventual presence of a tornado can occasionally be inferred based on a strong couplet near the ground. In this effort, the visual identification of a Tornado Vortex Signature (TVS; Brown and Wood, 2012), which corresponds to a change in wind speed and/or direction in

two adjacent individual pixels on radar display, is used here. Figure 7a identifies a small signature, represented by the vortex velocity pair composed of a yellow grid (outbound) and an adjacent slightly dark green grid (inbound), at the elevation EL = 0.7° inland, west-northwest of the mesocyclone, in the Doppler velocity field at 1147 UTC (indicated by the arrows in Fig. 7b).

This feature is weaker than that related to the mesocyclone, since the difference in adjacent outbound and inbound pixels is smaller. However, this does not imply that the rotation in the tornado is weaker than that in the mesocyclone: the latter may be the consequence of averaging a small vortex into a larger pixel. From a pixel-by-pixel analysis of the Doppler velocity at 1147 UTC, one may note that the value of TVS, represented by the difference of velocity in two adjacent pixels, is 14.6 m/s (inbound speed of 9.8 m/s and outbound speed of 4.8 m/s), which is closer to the Nyquist velocity V_N calculated earlier (equal to 11.76 m/s) than to $2V_N$. This means that it is not possible to smooth out this velocity gap if an even multiple of V_N is added or subtracted to the wind speed (Doppler velocity dealiasing). Thus, this velocity gap is true, suggesting the existence of a phenomenon with large velocity perturbation in a small area like a tornado.

The time evolution of the TVS can be better identified in the PPI along the two lower beams zoomed in the area near Sanremo (Fig. 8). A couple of adjacent pixels with different (inbound and outbound) directions is apparent at 1137 UTC at EL = 0.7° just in front of the coast. After 5 minutes, the signature can be identified at both elevation levels (EL = 0.7° and EL = -0.3°) just above the coastline near the city of Sanremo. Lastly, at 1147 UTC the signatures can be still found a few km inland, where the presence of a hook echo-like feature is also apparent. The frame sequence indicates that the vortices have moved north-northwestward, thus in a different direction compared to the mesocyclone, which has moved east-southeastward during the same period.

The locations of the subjectively specified TVS from 1137 to 1152 UTC every 5 minutes are shown all together in Fig. 9, at EL = 0.7° (red circles) and at EL = -0.3° (blue circles). The small vortex (TVS) in each PPI data was identified with the pair of adjacent Doppler velocity maximum and minimum in the area where the strong horizontal variations of velocity remained after velocity

data dealiasing. Although very close to each other, the two sets of circles at different elevations are not coincident.

For the TVS at 1137 UTC, the position at EL = 0.7° is relatively clear, whereas the TVS at EL = -0.3° near the same horizontal position is more uncertain due to the lack of wind data where there is no precipitation echo (bounded weak echo region). Due to the partially missing velocity data at EL = -0.3°, the reliability of the TVS at this time is lower, and for that reason it is identified as a dashed circle in Fig. 9.

The vortices at two different altitudes at 1147 UTC are not coincident, differently from the TVS at 1142 UTC. Considering the (coarse) spatial resolution of the radar data in the region, which is about 60 km far away from the radar site, inaccuracies in the position of the vortices due to the spatial resolution and also due to the PPI scan time difference of each elevation angle cannot be excluded a priori.

The temporal evolution of the characteristics of the TVS (diameter, tangential velocity, vertical component of vorticity) at these two elevation levels is shown on the lower panels of Fig. 9. The most intense phase of the vortex, characterized by a narrower diameter, higher values of velocity and of vertical vorticity, can be identified from 1137 to 1147 UTC at EL = 0.7°, and from 1142 to 1147 UTC at EL = -0.3°. During this phase: the diameter is similar at the two elevation levels, slightly reducing with time from about 1.1 km to 1.0 km; the tangential velocity at EL = 0.7° remains nearly constant at 7 m/s, while at EL = -0.3° it increases from 5.5 to 8.5 m/s; similarly, the vertical vorticity increases mainly at low levels, from 0.020 s^{-1} to 0.035 s^{-1}, while at EL = 0.7° the increase occurs from 1142 to 1147 UTC and is more limited, from 0.025 s^{-1} to 0.030 s^{-1}. The decay phase from 1147 to 1152 UTC corresponds to an increase of the TVS extent (diameter up to 1.9 km at EL = 0.7°, up to 1.4 km at EL = -0.3°) and a reduction of tangential velocity (down to 2.5 m/s at EL = 0.7°, to 4 m/s at EL = -0.3°) and vorticity (down to 0.005 s^{-1} at EL = 0.7°, to 0.012 s^{-1} at EL = -0.3°).

Figure 10 shows that the two circles denoting the locations of the TVS at 1137 UTC at different EL correspond well with the two locations where the passage of the vortices was reported after landfall by mass media and on the web. In particular, the yellow circle (EL = -0.3°) corresponds to the ground damages observed on the west side of the port area, while the white circle (EL = 0.7°) agrees well with the location where the second waterspout made landfall. The agreement is remarkable, considering that in the vicinity of Sanremo the range resolution is 500 m and the azimuth resolution is about 1 km. This suggests that the different rotational patterns identified at different elevation levels are really associated with different vortices and are not due to a parallax error.

Additional considerations can be drawn from Fig. 11, which shows the radial velocity convergence

calculated from the Doppler velocity data at 1152 UTC. The hatched area in the Figure identifies the convergence region, i.e. the extension of the area where the radial velocity divergence at EL = -0.3° is less than -0.002 s^{-1}. This zone closely matches the region with high radar reflectivity values on the southwestern side of the storm. From 1137 to 1152 UTC, the convergence zone and high radar reflectivity region moved in different directions, respectively northward and eastward (not shown); the TVS moved northward following the movement of the convergence zone. One may hypothesize that the convergence zone affected the development and movement of the small vortices at the time of their landing near Sanremo. This is consistent with Golden (1974), who discussed that the shear across a gust front may be a vorticity source for waterspout generation, and with Fujiwara and Fujiyoshi (2014), who proposed the vortices initially generated along the shear line of a gust front as an embryo for the genesis of waterspouts.

6. Conclusions

At least two waterspouts were reported near the city of Sanremo (northwestern Italy) at around 1230 Local Time (1130 UTC) on 1 December 2017, associated with a precipitation system moving

from the border of Italy and France northeastward near the Mediterranean coast. The waterspouts landed respectively in the center and in the port area of Sanremo city at around 1140 UTC, causing ground damage.

The Doppler radar analysis shows that a mesocyclone formed inside the strong echo region of the precipitation system and moved southeastward, unlike most of the surrounding echoes. Although the resolution was relatively coarse (500m and 1000m in the beamwise and azimuthal directions, respectively), two Doppler velocity couplets, identified as tornado vortex signatures, are apparent at two different elevations (-0.3° and 0.7°) from 1137 to 1152 UTC. The two features moved northward, corresponding well with the locations where the vortices were reported after landfall by mass media and websites.

Our interpretation is that the two waterspouts formed behind the strongest echo, developing in its southwestern side, possibly in the region of convergence separating the cooler air from the warm and moist inflow. This shear line may have affected the development and movement of the small vortices around the time of landing near Sanremo. While the strong echo with the mesocyclone moved southeastward (right-moving), the convergence line and the waterspouts moved toward the north, being decoupled from the strong echo, and decayed in a short time.

ACKNOWLEDGEMENTS

Agenzia Regionale per la Protezione dell'Ambiente Ligure (ARPAL) is gratefully acknowledged for providing the radar data. Doppler radar data analyses were performed using the Doppler radar analysis tool "Draft" developed by the Japanese Meteorological Research Institute (MRI). This study was supported in part by JSPS KAKENHI 18H01277.

REFERENCES:

Bech, J., Pascual, R., Rigo, T., Pineda, N., Lòpez, J.M., Arus, J., Gayà, M., 2007. An observational study of the 7 September 2005 Barcelona tornado outbreak. Nat. Hazards Earth Syst. Sci. 7, 129–139.

Bluestein, H. B., 1985: The formation of a ‘‘landspout’’ in a ‘‘brokenline’’ squall line in Oklahoma. Preprints, 14th Conf. on Severe Local Storms, Indianapolis, IN, Amer. Meteor. Soc., 267–270.

Brown, R.A., Wood, V.T., 2012. The tornadic vortex signature: An update. Weather Forecast. 27, 525-530.

Buzzi, A., Davolio, S., Malguzzi, P., Drofa, O., Mastrangelo, D., 2014. Heavy rainfall episodes over Liguria of autumn 2011: Numerical forecasting experiments. Nat. Hazards Earth Syst. Sci. 14, 1325–1340.

Cassola, F., Ferrari, F., Mazzino, A., Miglietta, M.M., 2016. The role of the sea on the flash floods events over Liguria (northwestern Italy). Geophys. Res. Lett. 43, 3534-3542, doi:10.1002/2016GL068265.

Collins, W.G., Paxton, C.H., Golden, J.H., 2000. The 12 July 1995 Pinellas County, Florida, tornado/waterspout. Weather Forecast. 15, 122-134.

Fiori, E., Comellas, A., Molini, L., Rebora, N., Siccardi, F., Gochis, D.J., Tanelli, S., Parodi A., 2014. Analysis and hindcast simulation of an extreme rainfall event in the Mediterranean area: The Genoa 2011 case. Atmos. Res. 138, 13–29.

Fujiwara, C., Fujiyoshi, Y., 2014. Detection of “invisible waterspout” using 3D scanning Doppler lidar. SOLA 10, 127-130.

Giaiotti, D. B., Giovannoni, M., Pucillo, A., Stel F., 2007. The climatology of tornadoes and waterspouts in Italy. Atmos. Res. 83, 534–541.

Golden, J.H., 1974a. The life cycle of Florida Key’s waterspouts. I. J. Appl. Meteorol. 13, 676−692.

Golden, J.H., 1974b. The life cycle of Florida Key’s waterspouts. II. J. Appl. Meteor. 13, 693−709.

Golden, J.H., Sabones, M.E., 1991. Tornadic-waterspout formation near intersecting boundaries. Preprints, 25th International Conference on Radar Meteorology, 420-423, American Meteorological Society, Boston.

Huuskonen, A., Saltikoff, E., Holleman, I., 2014. The Operational Weather Radar Network in Europe. Bull. Am. Meteorol. Soc. 95, 897–907.

Kato, R., Kusunoki, K., Inoue, H.Y., Arai, K., Nishihashi, M., Fujiwara, C., Shimose, K., Mashiko, W., Sato, E., Saito, S., Hayashi, S., Yoshida, S., Suzuki, H., 2015. Modification of misovortices during landfall in the Japan Sea coastal region, Atmos. Res. 158–159, 13–23.

Lee, B.D., Wilhelmson, R.B., 1997a. The Numerical Simulation of Non-Supercell Tornadogenesis, Part I: Initiation and Evolution of Pretornadic Misocyclone Circulations along a Dry Outflow Boundary. J. Atmos. Sci. 54, 32-60.

Lee, B.D., Wilhelmson, R.B., 1997b. The numerical simulation of non-supercell tornadogenesis. Part II: Evolution of a family of tornadoes along a weak outflow boundary. J. Atmos. Sci. 54, 2387–2415.

Markowski, P. M., 2002. Hook Echoes and Rear-Flank Downdrafts: A Review. Mon. Weather Rev. 130, 852–76.

Markowski, P.M., Richardson, Y., 2010. Mesoscale Meteorology in Midlatitudes. Wiley-Blackwell, 424 pp.

Matsangouras, I. T., Nastos, P. T., Bluestein, H. B., Papachristopoulou, K., Pytharoulis, I., Miglietta, M. M., 2017. Analysis of waterspout environmental conditions and of parent-storm behaviour based on satellite data over the southern Aegean Sea of Greece. Int. J. Clim. 37, 1022–1039

McDonald, J., Mehta, K.C., 2006. A recommendation for an enhanced Fujita scale (EF-scale), revision 2. Wind Science and Engineering Research Center Rep., Texas Tech University, 111 pp. [Available online at http://www.spc.ncep.noaa.gov/efscale/ef-ttu.pdf]

Miglietta, M.M., Rotunno, R., 2016. An EF3 multivortex tornado over the Ionian region: Is it time for a dedicated warning system over Italy? Bull. Am. Meteorol. Soc. 97, 337–344.

Miglietta, M.M., Mazon, J., Rotunno, R., 2017a. Numerical simulations of a tornadic supercell over the Mediterranean. Weather Forecast. 32, 1209–1226.

Miglietta, M.M., Mazon, J., Motola, V., Pasini, A. 2017b. Effect of a positive sea surface temperature anomaly on a Mediterranean tornadic supercell. Scientific Reports 7(12828), 1–8.

Miglietta M.M., Matsangouras, I.T., 2018. An updated "climatology" of tornadoes and waterspouts in Italy. Int. J. Clim. 38, 3667-3683.

Renko, T., Kuzmic, J., Soljan, V., Strelec Mahovic, N., 2016. Waterspouts in the Eastern Adriatic from 2001 to 2013. Natural Hazards 82, 441–470.

Rodríguez, O., Bech, J., 2018. Sounding-derived parameters associated with tornadic storms in Catalonia. Int. J. Clim. 38, 2400–2414.

Saha, S., and Coauthors, 2010. The NCEP Climate Forecast System Reanalysis. Bull. Amer. Meteor. Soc. 91, 1015-1057.

Simmons, K.M., Sutter, D., 2011. Economic and societal impact of tornadoes (282 pp.). Boston, MA: American Meteorological Society Press.

Simpson, J., Morton, B.R., McCumber, M.C., Penc, R.S., 1986. Observations and mechanisms of GATE waterspouts. J. Atmos. Sci. 43, 753-782.

Sioutas, M.V., Keul, A.G., 2007. Waterspouts of the Adriatic, Ionian and Aegean Sea and their meteorological environment. Atmos. Res. 83, 542–557.

Sioutas, M., Szilagyi, W., Keul, A., 2013. Waterspout outbreaks over areas of Europe and North America: environment and predictability. Atmos. Res. 123, 167–179.

Sugawara, Y., Kobayashi, F., 2008. Structure of a waterspout occurred over Tokyo Bay on May 31 2007. SOLA 1, 1-4.

Tibaldi, S., Buzzi A., Malguzzi, P., 1980. Orographically induced cyclogenesis: Analysis of numerical experiments. Mon. Wea. Rev., 108, 1302-1314.

Tochimoto, E., Niino, H., 2016. Structural and environmental characteristics of extratropical cyclones that cause tornado outbreaks in the warm sector: a composite study. Mon. Wea. Rev., 144, 945-969.

Tochimoto, E., Niino, H., 2018. Structure and Environment of Tornado-Spawning Extratropical Cyclones around Japan. J. Meteorol. Soc. Japan, 96, 355-380.

Van Den Broeke, M.S., Van Den Broeke, C.A., 2015. Polarimetric radar observations from a waterspout-producing thunderstorm. Weather Forecast. 30, 329–348.

van Tassel, E. L., 1955: The North Platte Valley tornado outbreak of June 27, 1955. Mon. Wea. Rev., 83, 255–264.

Verlinde, J., 1997. Airborne Doppler radar analysis of a TOGA COARE waterspout storm. Mon. Weather Rev. 125, 3008–3017.

Wakimoto, R.M., Lew, J.K., 1993. Observations of a Florida waterspout during Cape. Weather Forecast. 8, 412–423.

Wakimoto, R.M., Wilson, J.W., 1989. Non-supercell tornadoes. Mon. Weather Rev. 117, 1113-1140.

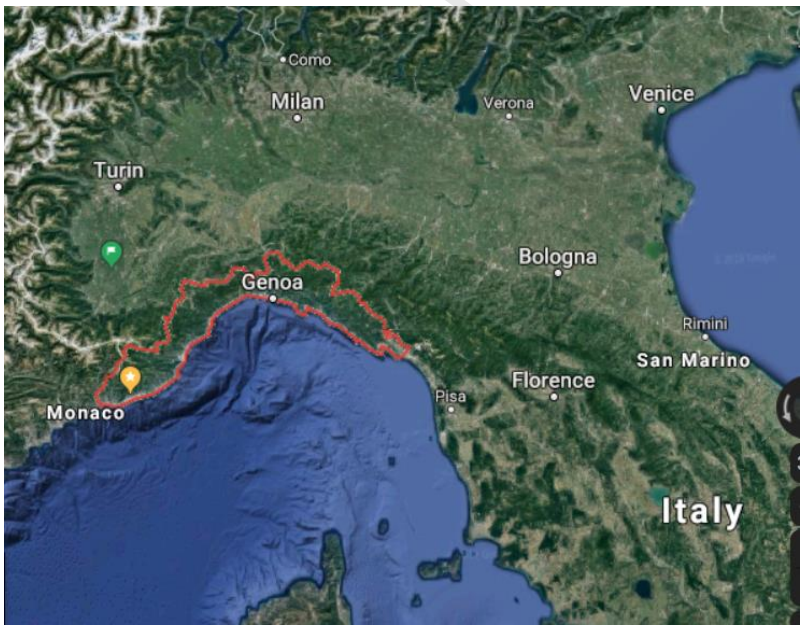

Figure 1: topography of the area surrounding Sanremo (yellow mark), Liguria region (geographic and political borders denoted with a red contour) and location of the radiosounding station of Cuneo Levaldigi (green mark). Imagery@2019 Landsat / Copernicus, Data SIO, NOAA, U.S. Navy, NGA, GEBCO, Map data @2019 GeoBasis-DE/BKG (@2009), Google, Inst. Geogr. Nacional.

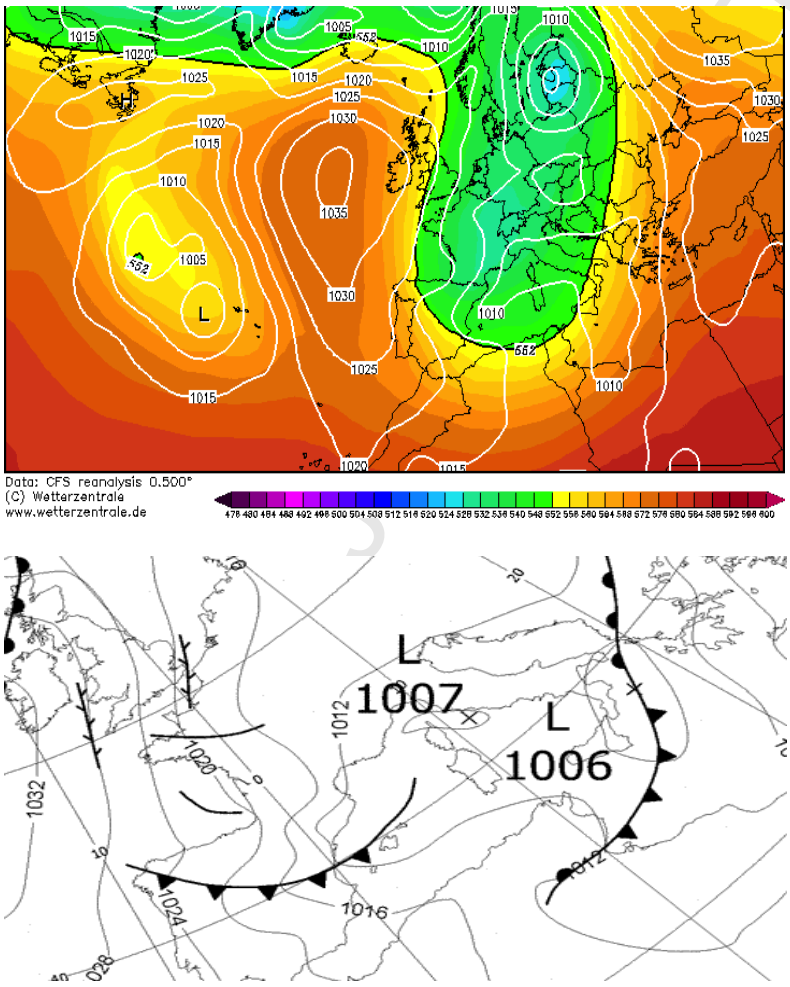

Figure 2: Climate Forecasting System (CFS) reanalysis at 1200 UTC, 1 December 2017 (500 hPa geopotential height in gpdam, colors; mean sea level pressure in hPa, white contours) (top);

Bracknell weather map (mean sea level pressure in hPa -contours-, and fronts) at 1200 UTC, 1 December 2017, zoomed in the western Mediterranean (bottom) (source: www.wetterzentrale.de; www1.wetter3.de).

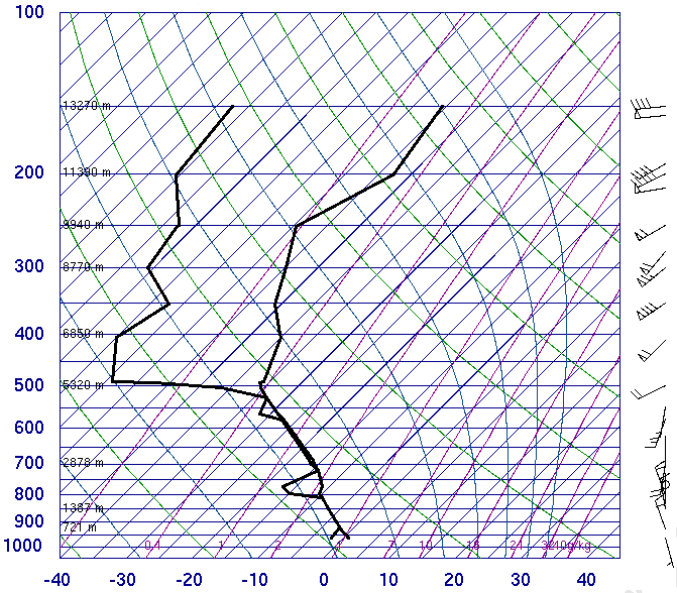

Figure 3: Cuneo Levaldigi skew-T diagram at 1200 UTC, 1 December 2017 (source: http://weather.uwyo.edu).

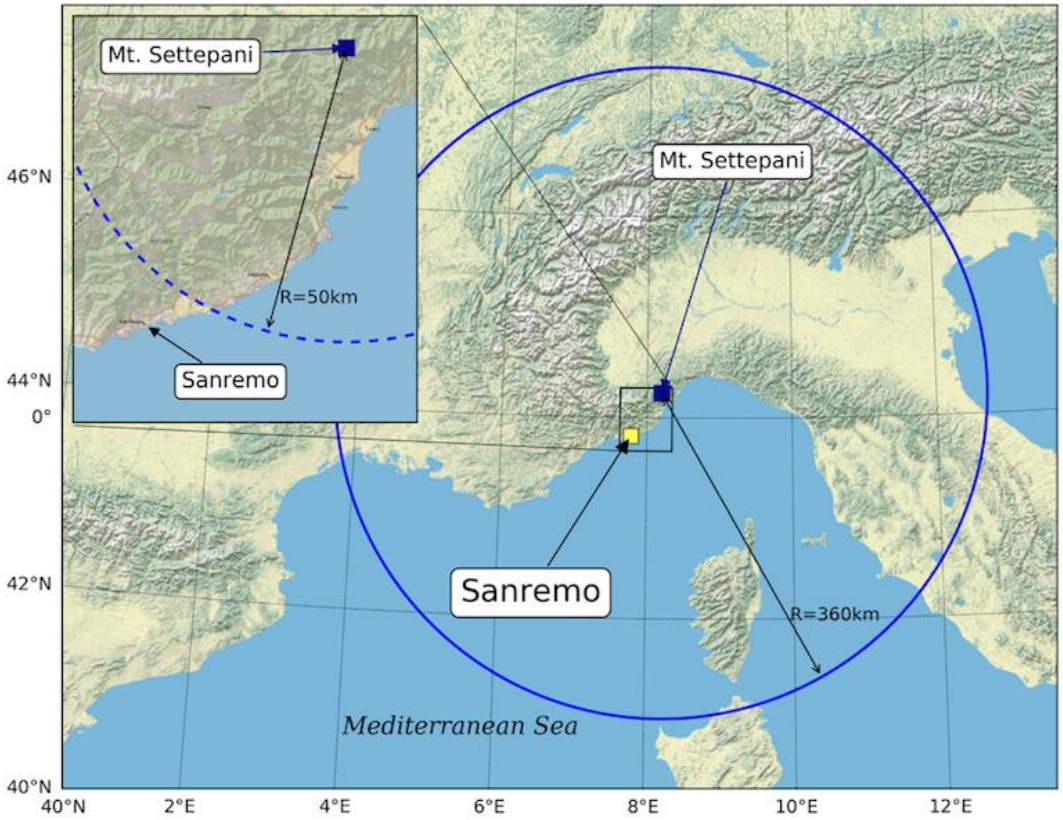

Figure 4: location of the Settepani radar and Sanremo city (zoomed in the left upper corner).

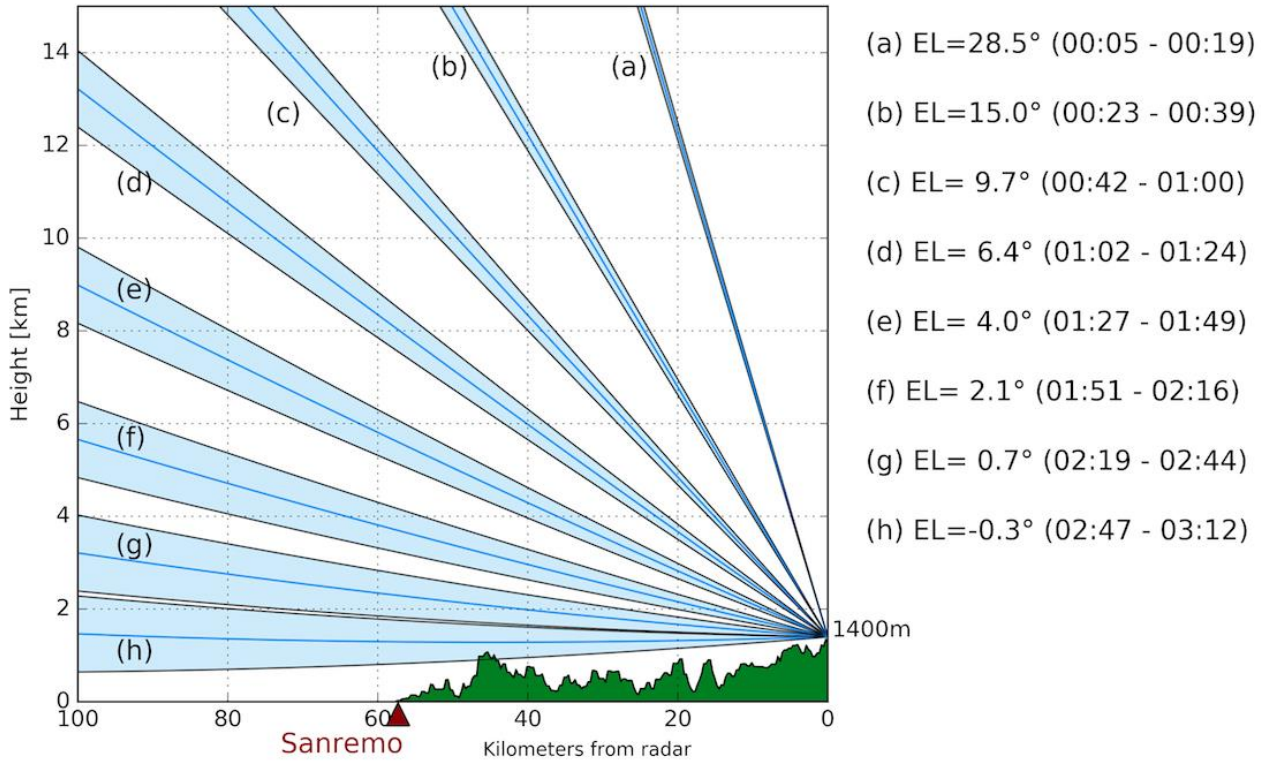

Figure 5: Time for volume scanning every 5 minutes at 8 different elevation angles in Settepani radar. The topographic profile from Monte Settepani radar site to Sanremo is shown in the bottom.

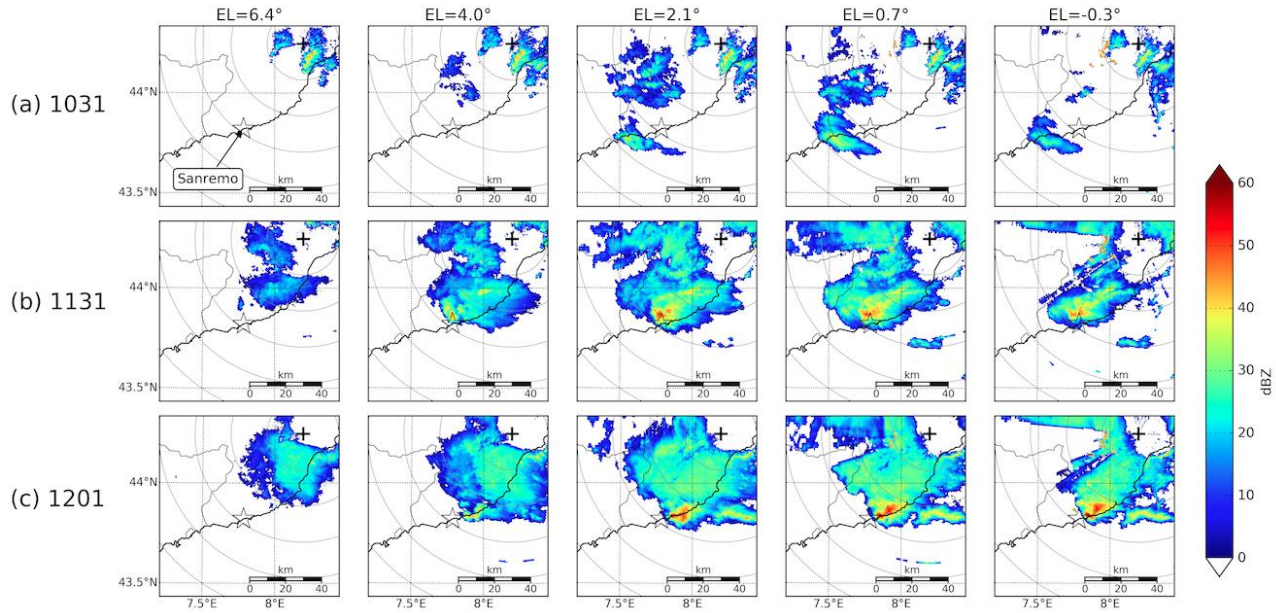

Figure 6: plan position indicator (PPI) scans at EL = 6.4°, 4.0°, 2.1°, 0.7°, - 0.3° (from left to right), at 1031 UTC (top), 1131 UTC (middle), 1201 UTC (bottom). The star denotes the location of Sanremo.

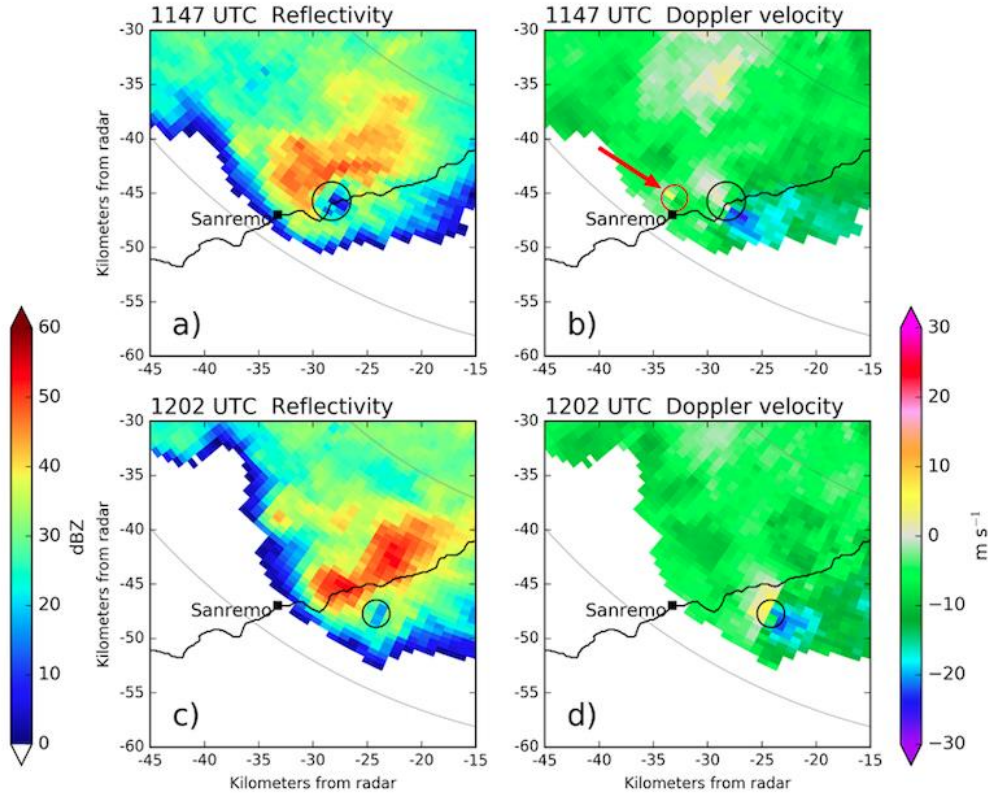

Figure 7: PPI at 0.7° elevation angle with starting azimuth of 87.5° (left) and Doppler radar data after dealiasing (right) at 1147 UTC (a, top) and at 1202 UTC (b, bottom). The black circle identifies the subjectively identified mesoscale vortex. The distance in km from the radar site is shown in the two axes. The arrows identify an outbound velocity pixel within an inbound extensive region.

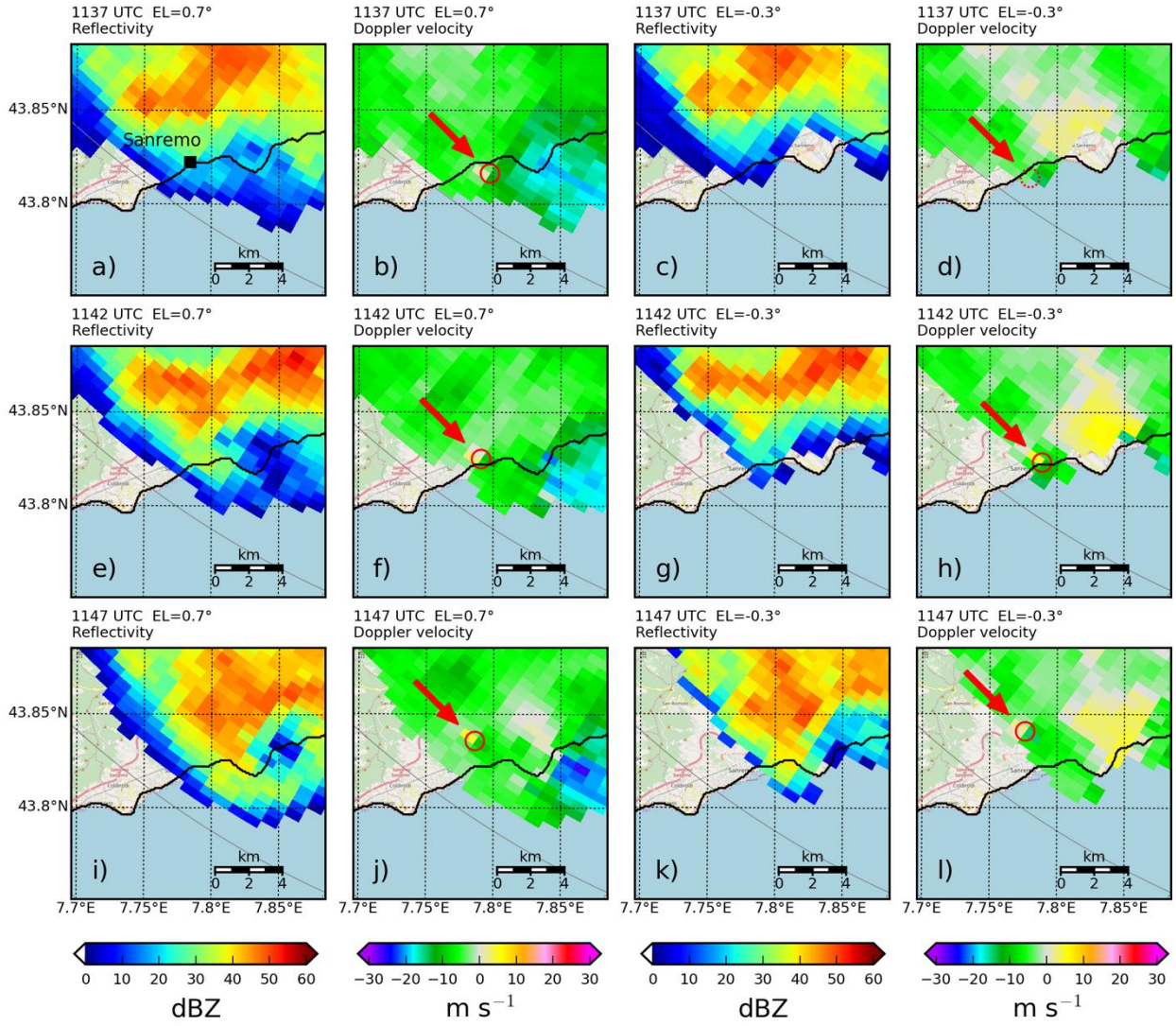

Figure 8: PPI reflectivity (first and third column) and Doppler radar data (second and forth column) at 0.7° (left half) and -0.3° elevation angle (right half) at around 1137 UTC (a, top), 1142 UTC (b, middle), 1147 UTC (c, bottom). The TVS signature is identified with the red circle and the arrow.

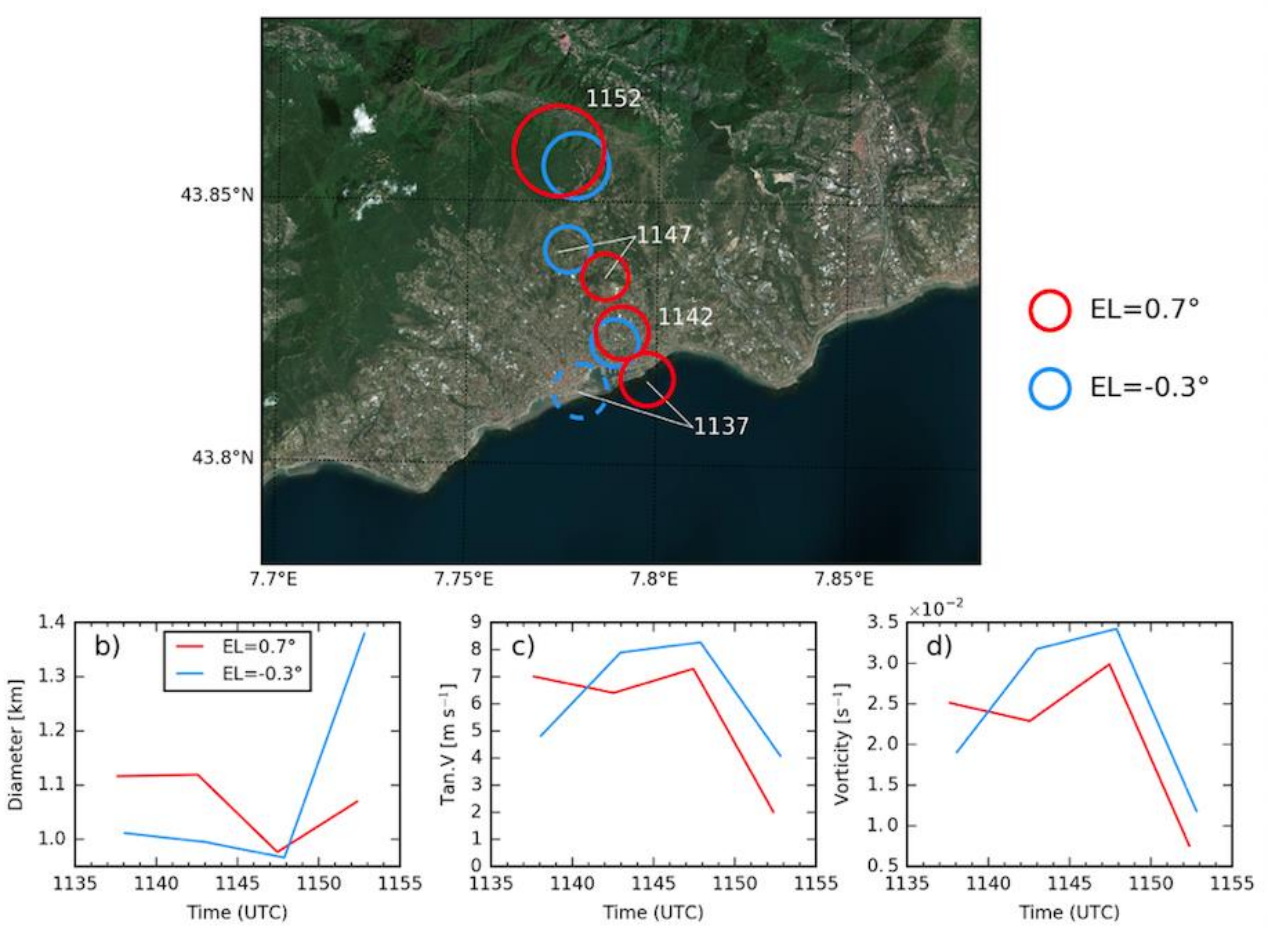

Figure 9: location of the subjectively identified TVS from 1137 to 1152 UTC every 5 minutes, at EL = 0.7°, i.e. around 2250 a.s.l.m. near Sanremo (red circles), and at EL = -0.3°, i.e. around 1300 a.s.l.m. near Sanremo (blue circles). Lower inset: Diameter (left), tangential velocity (middle) and vertical vorticity (right) of the subjectively identified vortices (red for EL = 0.7°, blue for EL = -0.3°) as a function of time (in UTC).

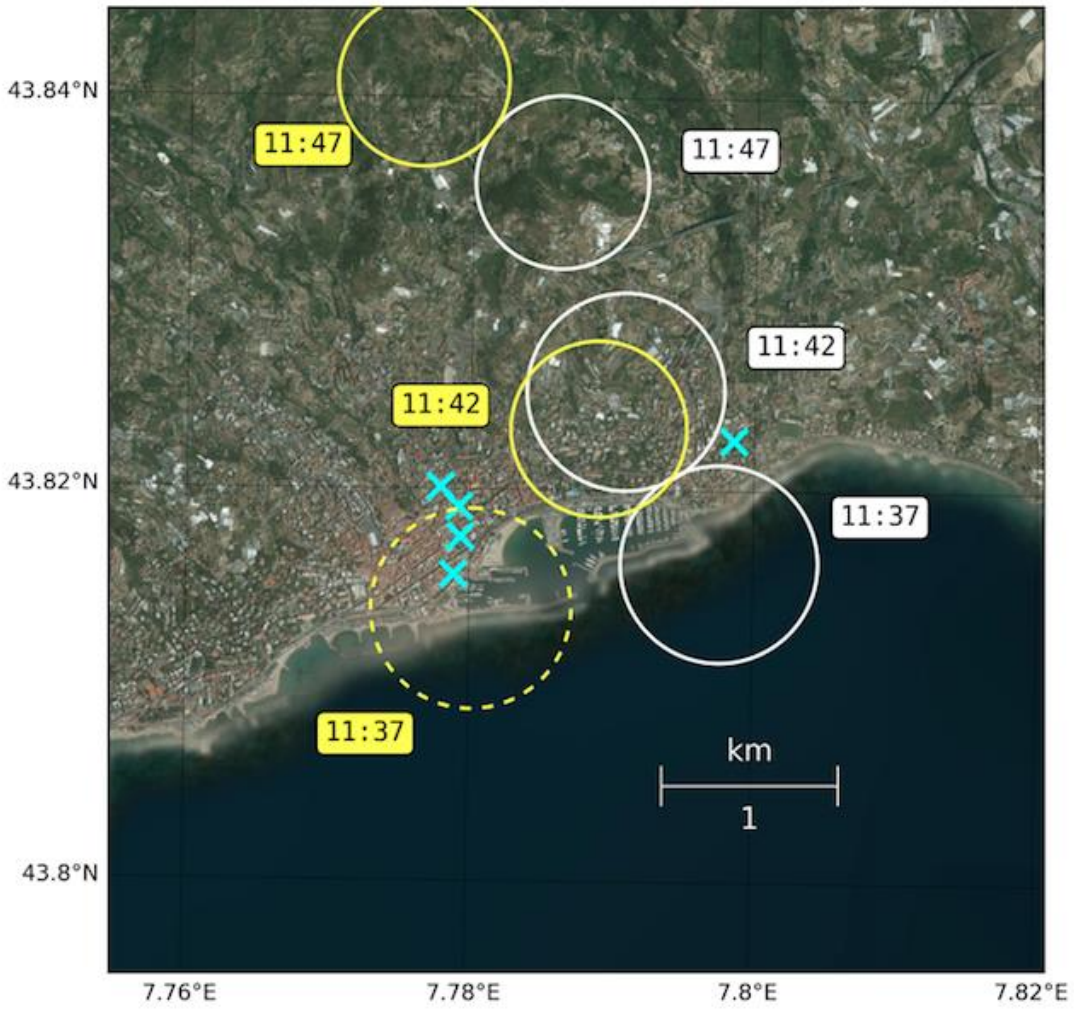

Figure 10: location of the subjectively identified TVS at EL = 0.7° (white circles) and at EL = -0.3° (yellow circles) in the port area of Sanremo. The cyan crosses identify the area where most damages were reported.

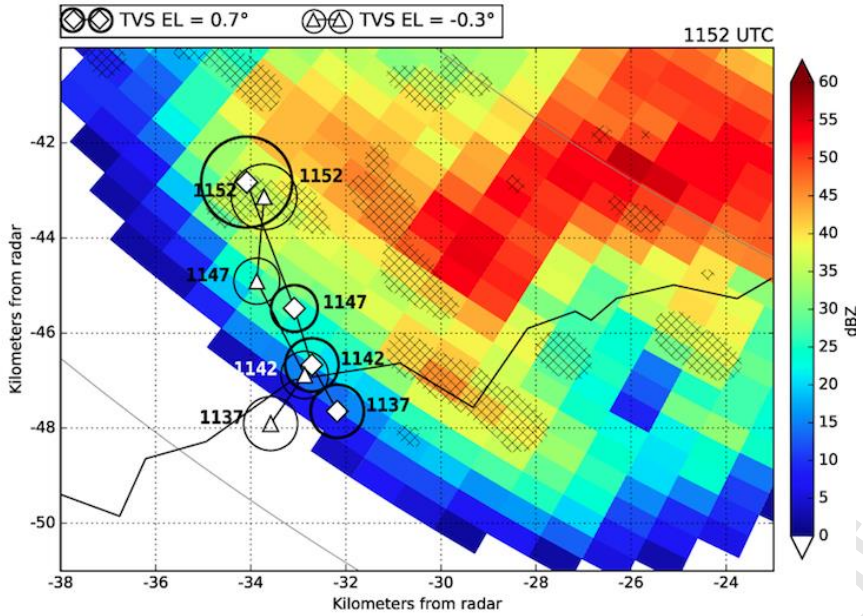

Figure 11: radial velocity convergence (hatched area for divergence less than -0.002 m s^{-1}) at EL =-0.3°, at 1152 UTC. Also shown are: radar reflectivity (dBZ) at EL = 0.7° (shaded), diamond markers with thick circle (TVS at EL = 0.7°, from 1137 to 1152 UTC, every 5 minutes), triangle markers with thin circle (TVS at EL = -0.3°, from 1137 to 1152 UTC, every 5 minutes),

HIGHLIGHTS

- Two waterspouts in the Mediterranean Sea are analyzed with a C-band Doppler radar.
- A mesocyclone and a velocity couplet at two different elevations are identified.
- The waterspouts developed in the region of convergence of cooler and warmer air.